Journal of Alloys and Compounds 713 (2017) 222–228

Contents lists available at ScienceDirect

Journal of Alloys and Compounds

journal homepage: http://www.elsevier.com/locate/jalcom

Microstructural characterization and properties of Ti-28Ta at.% powders produced by plasma rotating electrode process

J.O. Yin [a], G. Chen [a, b, *], S.Y. Zhao [a], Y. Ge [a], Z.F. Li [a], P.J. Yang [c], W.Z. Han [c], J. Wang [a], H.P. Tang [a, d, **], P. Cao [e]

[a] State Key Laboratory of Porous Metal Materials, Northwest Institute for Non-ferrous Metal Research, Xi'an, Shaanxi, 710016, PR China
[b] State Key Laboratory of Powder Metallurgy, Central South University, Changsha, Hunan, 410083, PR China
[c] State Key Laboratory for Mechanical Behavior of Materials, Xi'an Jiaotong University, Xi'an, Shaanxi, 710049, PR China
[d] Xi'an Sailong Metal Materials Co. Ltd., Xi'an, Shaanxi, 710016, PR China
[e] Department of Chemical and Materials Engineering, The University of Auckland, Auckland, 1142, New Zealand

ARTICLE INFO

Article history:
Received 25 January 2017
Received in revised form
16 April 2017
Accepted 18 April 2017
Available online 19 April 2017

Keywords:
Plasma rotating electrode process (PREP)
Ti-Ta alloy
Rapid solidification
Martensitic transformation

ABSTRACT

Ti-28 at.%Ta powders were produced by rapid solidification *via* plasma rotating electrode process (PREP). It is found that microstructure, morphology and phase constituents of Ti-28Ta powders are particle size dependent. Small powder particle exhibit the formation of predominant martensitic α" and minor metastable β, whilst large particles consist of primary metastable β with minor martensitic α" phase. The amount of martensitic α" increases while the amount of metastable β phase decreases with decreasing the particle size. The martensitic α" lath with the size of about 50 nm wide and 1 μm long are formed preferentially at the β grain boundaries. The martensitic transformation start temperature (M_s) and peak temperature (M_p) are ~390 °C and ~340 °C respectively for the Ti-28Ta powders with the particle size between 40 and 65 μm. An increased Vickers micro-hardness is obtained and is associated with decreasing particle size.

1. Introduction

Ti-Ta alloys are considered to be among the best biomaterials because of their excellent biocompatibility and lower elastic modulus as compared to other titanium alloys [1–5]. Additive manufacturing has been becoming a primary manufacturing method for titanium based biomedical devices and implants in recent years. Spherical powders of titanium-based alloys with suitable particle size distribution (PSD) are urgently required to be used in additive manufacturing processes. In this context, nowadays atomization *via* plasma rotating electrode process (PREP) is a suitable technique for the synthesis of high-purity powders of reactive metals with high melting point such as high-quality titanium and titanium alloys powders [6–8]. During atomization, liquid droplets are tangentially emitted by centrifugal force and finally solidified into spherical particles. In the Ti-Ta system, upon quenching, primary β transforms to orthorhombic α". The other phases include, depending on the composition, α' – an HCP martensitic phase, metastable Ti-rich β that is retained from high temperature and athermal ω phase [9]. It was reported that phase transformations from β to martensitic α" or athermal ω are critically dependent on cooling [4,10]. Controlling these two martensitic phases in Ti-Ta alloys is important to achieve desired shape memory properties [4]. For Ti-28Ta (Ti-60 wt%Ta), Margevicius and Cotton [10] reported that the volumetric fraction of athermal ω increases with the pre-quenching temperature. Zhou et al. [2] observed a large amount of retained β and a small amount of α" but no athermal ω in their study when they water quenched the bulk Ti-28Ta alloy from 1000 °C. It is generally agreed that in addition to the alloy composition, the cooling rate during the quenching plays a significant role in determining the phase evolution of Ti-Ta alloys. In most of the previous studies, only limited cooling rates were obtained by applying conventional quenching processes [2,4,10]. On the other hand, the accessible cooling rate in PREP can be as high as 10^4~10^6 K/s [11]. Such high cooling rates may lead to the microstructures and phase constituents that are not

* Corresponding author. State Key Laboratory of Porous Metal Materials, Northwest Institute for Non-ferrous Metal Research, Xi'an, Shaanxi, 710016, PR China.
** Corresponding author. State Key Laboratory of Porous Metal Materials, Northwest Institute for Non-ferrous Metal Research, Xi'an, Shaanxi, 710016, PR China.
E-mail addresses: mychgcsu@163.com (G. Chen), hptang@c-nin.com (H.P. Tang).

http://dx.doi.org/10.1016/j.jallcom.2017.04.195
0925-8388/

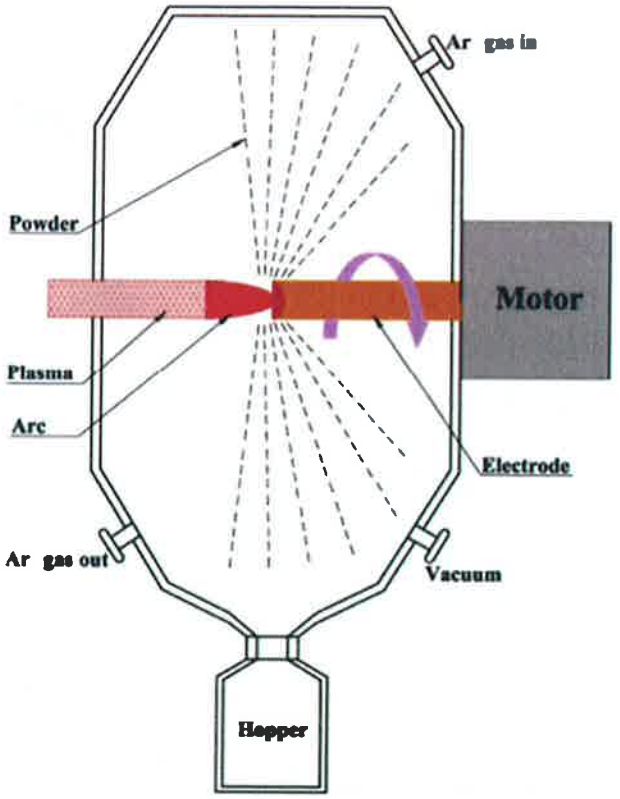

Fig. 1. Schematic illustration of the plasma rotating electrode process (PREP).

observed in the conventional quenching treatments for the Ti-Ta alloys.

In this study, we report the micro-morphologies, the phase constituents, and the mechanism of martensitic transformation of Ti-28Ta powders produced *via* PREP. We were particularly interested in establishing how the particle size relates to the characteristics of the PREP Ti-28Ta powders.

2. Experimental

Ti sponge and Ta powders in a nominal composition ratio of Ti-28 at.%Ta were melted in an arc melting furnace. The Ti-28Ta ingot was casted after melting five times, followed by forging at 950 °C. A rod of 50 mm in diameter was shaped and used as the PREP anode. The spherical Ti-28Ta powders were subsequently produced by PREP (SLPREP-1, Sailong Metal Co. Ltd. P.R. China), as shown in Fig. 1. In the PREP process, the anode, which rotated at 12000 rpm, was melted by an electric arc at a constant DC current of 1100 A. Then, the liquid droplets were emitted due to the centrifugal force and further atomized and solidified into spherical particles owing to the surface tension [6].

The flowability and apparent density of Ti-28Ta powders were determined by using a Hall flowmeter, as per the ASTM B213-13 for flow-rate measurements and ASTM B212~13 for apparent density measurements. Phase constituents were determined by X-ray diffraction (XRD, Bruker D8 Advance Phaser). Microstructure and morphology of the Ti-28Ta powders were observed by optical microscopy (OM, Leica DM2500M), scanning electron microscopy (SEM, JEOL JSM6460) and transmission electronic microscopy (TEM, JEOL2100F). TEM foil specimens were sectioned by focused ion beam (FIB, FEI Helios NanoLab DualBeam). Fig. 2 shows the detailed procedure of foil preparation for TEM using FIB. Firstly, one Ti-28Ta powder with the diameter of *ca.* 40 μm shown in Fig. 2(a) was selected for sectioning. Subsequently, the desired thin foil was sectioned and then mounted to a micromanipulator by deposition of platinum, Fig. 2(b)–(e). Finally, the foil was further thinned by FIB for the following TEM observations. Phase transformation temperatures of Ti-28Ta powders were determined by differential scanning calorimetry (DSC, NETZSCH DSC 204F1) with a heating-and-cooling rate of 10 K/min. Vickers micro-hardness for the individual powder particles with various particle sizes was measured using a load of 0.098N (10gf).

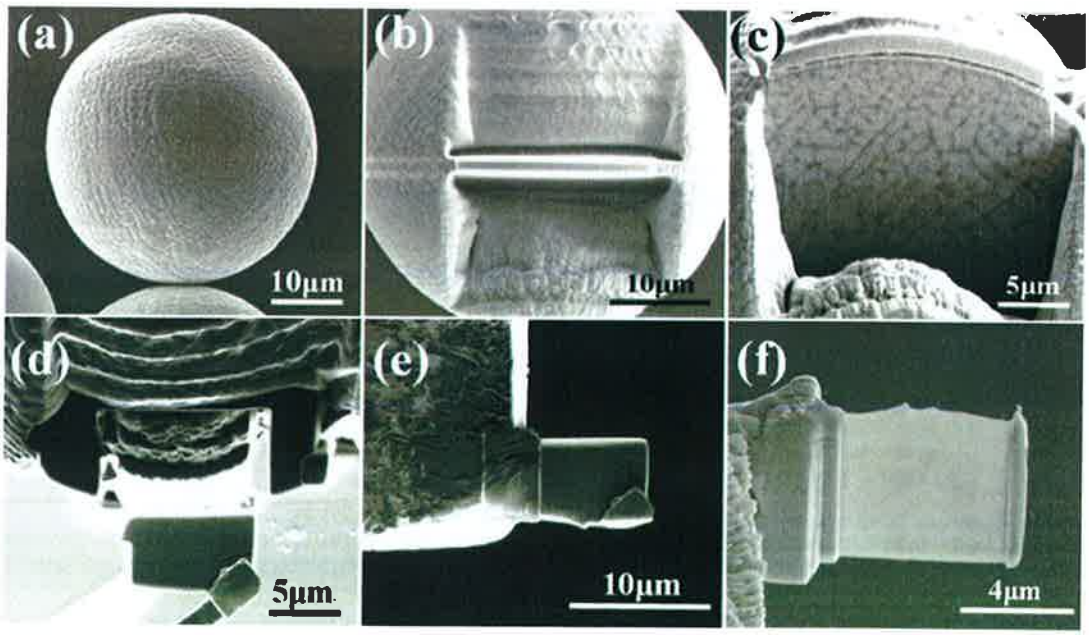

Fig. 2. Sample preparation by FIB for TEM observations (a) a selected Ti-28Ta powder particle, (b) foil sectioning, (c) bulking out, (d) lifting out, (e) mounting and (f) final thinning.

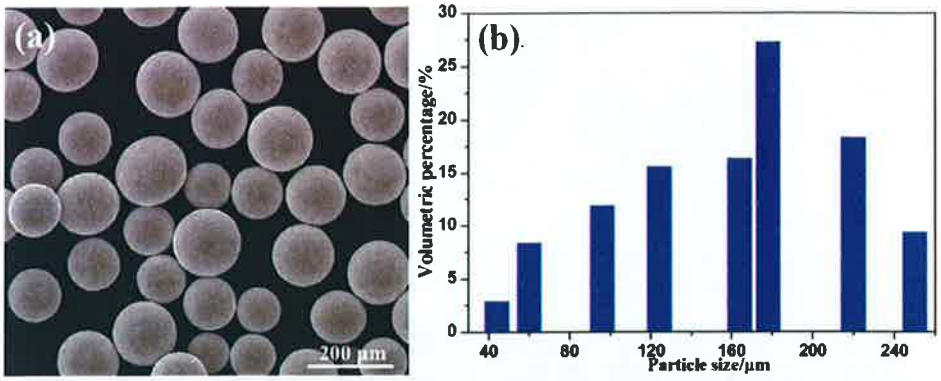

Fig. 3. (a) SEM micrograph of the PREP Ti-28Ta powders and (b) particle size distribution.

3. Results

3.1. Powder morphology

Fig. 3(a) shows the surface micrographs of the PREP Ti-28Ta powders. In general, the spherical Ti-28Ta particles exhibit smooth surface appearance and no satellite particles are found. The expected spherical particle morphology is a result of surface tension during the rapid solidification. The combination of high sphericity and non-satellite particles contributes to its good powder flowability, *i.e.*, 15.5 s/50 g. A wide particle size distribution of 30–260 μm was observed, as shown in Fig. 3(b). It was reported that the particle size distribution for the PREP powders largely depends on the processing parameters such as the rotating speed, electrode diameter and DC current [12]. The PREP Ti-28Ta powders were classified into three batches according to their variable particle size ranges, *i.e.*, 150–178, 89–124, 40–65 μm. These batches are referred to as large, medium and small powders, respectively.

Surface morphology and cross-sectional microstructure of the Ti-28Ta powders are displayed in Fig. 4. The large powders (>150 μm), as shown in Fig. 4(a), reveal the rough surface morphology of equiaxed dendrite. Fig. 4(b) shows a cross section of a large particle, where smaller dendrites can be found at the outer layer but larger equiaxed dendrite is located in the center region on the cross section. With decreasing the particle size, the powder surface becomes smooth, Fig. 4(c) and fine equiaxed and orthogonal dendrites are clearly observed from the surface and internal morphologies of powders with the particle size of 89–124 μm, Fig. 4(c) and (d). The equiaxed dendrite morphology with long dendrite arms is the characteristic feature of the growth of cubic β phase from the liquid during the rapid solidification [13]. With further reduction of the particle size to 40–65 μm, the particle surface becomes smooth (Fig. 4(e)), while its internal microstructure reveals a typical finer orthogonal dendrite morphology, Fig. 4(f). Similar phenomenon has been also observed in the PREP TiAl alloy powders [8]. This is mainly attributed to the much higher cooling rate for small powders as compared to the large particles. It has been reported that the typical cooling rate of powders for titanium alloys is estimated to be 10^4~10^6 K/s [11]. Because of the high cooling rate and small thermal mass during the rapid solidification process, time available for the diffusion or orientation in the titanium powders is not high enough. The powder particle is so small that the surface shrinkage induced by the cooling would not make enough stress to create enough separation of the surface skin [14].

3.2. Phase constituents

Fig. 5 shows XRD patterns of the raw material and PREP powders as a function of particle size. The raw rod for PREP consists of major β with minor α" phase as shown in Fig. 5(a). However, the XRD patterns of the powders show that their phase constituents are significantly dependent on the particle size. For instance, in Fig. 5(b), larger powders (150–178 μm) exhibit predominant β phase coexistent with a minor α". In fine powders (40–65 μm), α" becomes another major phase in addition to the retained β phase, (Fig. 5(d)). The intensities of the diffraction peaks for α" (020), (022) and (110) increase with decreasing particle size. In other words, this implies that smaller particles contain more martensitic α" but less β.

To further confirm the XRD analysis, TEM was conducted to analyze the phases of the powders. Fig. 6 shows the TEM images and selected area electron diffraction (SAED) pattern taken at the area of Fig. 6(b) for the fine powder with the particle size of 40–65 μm. It can be observed in Fig. 6(a) that the microstructure of the Ti-28Ta powders is composed of fine grains with the size of *ca.* 1 μm. Interestingly, the needle-like martensitic α" phase in Fig. 6(b), which is indexed by SAED in Fig. 6(c), is found to be located at the grain boundaries, while the matrix of the grain in Fig. 6(b) is determined to be β phase. The corresponding SAED (Fig. 6(c)) well agrees with the XRD results in Fig. 5(d). This indicates that the martensitic α" is preferentially formed at the grain boundaries during rapid solidification in the present study. Nevertheless, this phenomenon is different from the results in previous studies on bulk Ti-Ta alloys with compositions around Ti-28Ta [2,7,10], in which martensitic α" phase was formed within the grain matrix rather than at the grain boundary. In these studies, the width of the martensitic α" plate ranges from hundreds of nanometers to several micrometers [4,10]. However, in the present study, Fig. 6(b) reveals the martensitic width is less than 50 nm, which is significantly smaller than that in the bulk Ti-28Ta alloy [10]. Besides, the length of the martensitic α" plate here is below 1 μm.

3.3. Phase transformation temperature

Fig. 7 shows the DSC curves upon heating and cooling for the fine Ti-28Ta powders (40–65 μm). An endothermic peak upon heating was observed, indicating a martensite-to-austenite transition. The transformation temperatures are estimated from the DSC curve with the austenite starting temperature (A_s) ~421 °C, austenite finishing temperature (A_f) ~593 °C and austenite peak

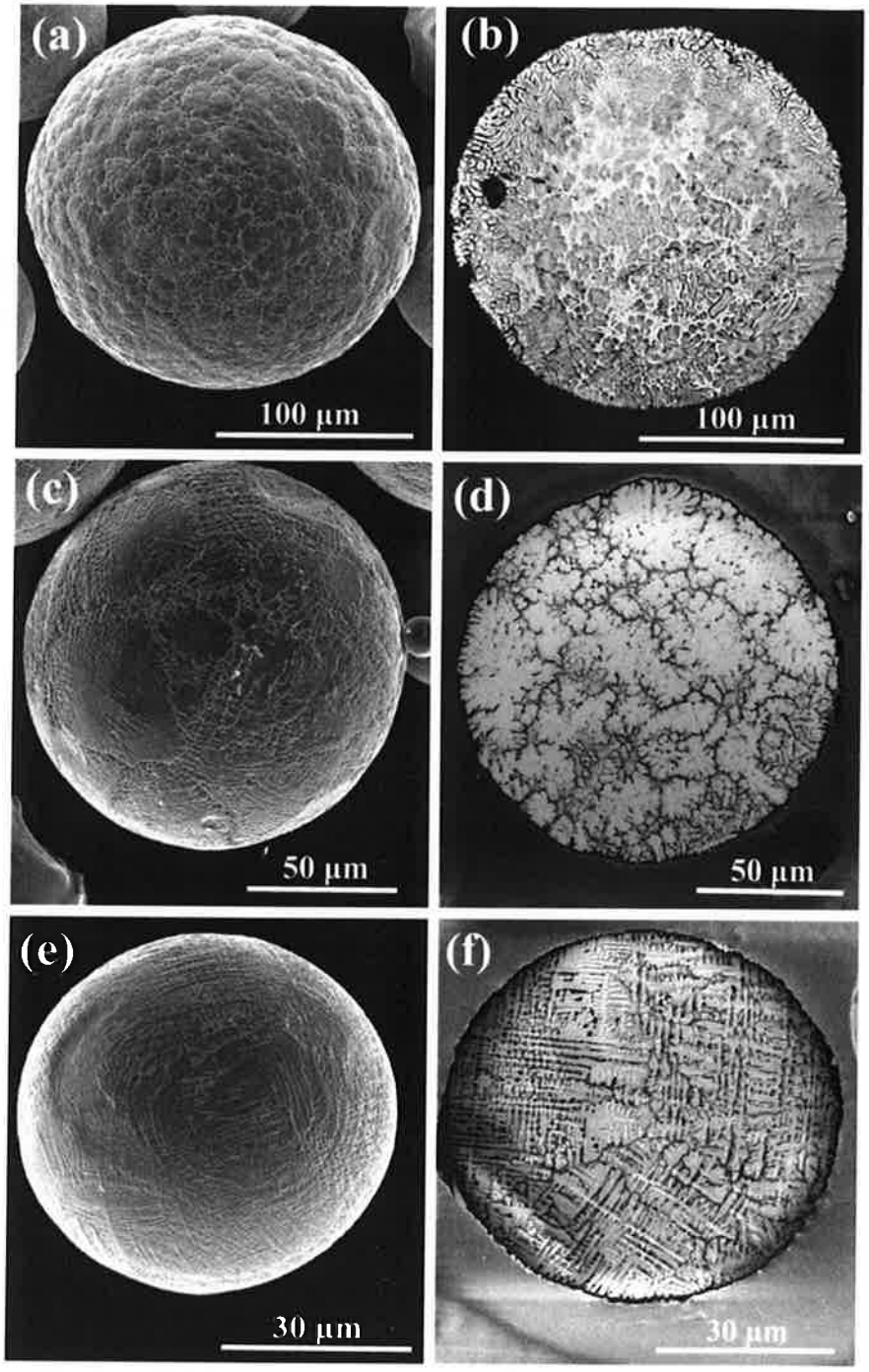

Fig. 4. Micrographs of the PREP Ti-28Ta powders with the particle size range of (a) and (b) 150–178 μm, (c) and (d) 89–124 μm, (e) and (f) 40–65 μm (a), (c) and (d) surface morphologies, while (b), (d) and (f) are cross-sectional views.

temperature (A_p) ~540 °C. In comparison with the data for a bulk Ti-15Ta alloy [15], the A_p temperature of the Ti-28Ta powders decreases by about 240 °C. It is commonly recognized that the addition of Ta can stabilize β phase and decrease the martensite-to-austenite transformation temperature [4]. Furthermore, a weak exothermic peak associated with martensite formation, is found upon cooling. A similar result was also reported for the Ti-30Nb-3Pd alloy [16]. The martensitic start temperature (M_s) is estimated to be ~390 °C, martensitic finish temperature (M_f) ~253 °C and martensitic peak temperature (M_p) ~340 °C, respectively. It should be noted that sufficient amount of Ta addition could suppress the martensitic transformation. No martensitic peak in bulk Ti-Ta alloys with composition around Ti-28Ta were observed, which is attributed to the low enthalpy of the transformation from β to martensitic α" [15,17]. Similar phenomenon was also reported for some other Ti alloys [18–21].

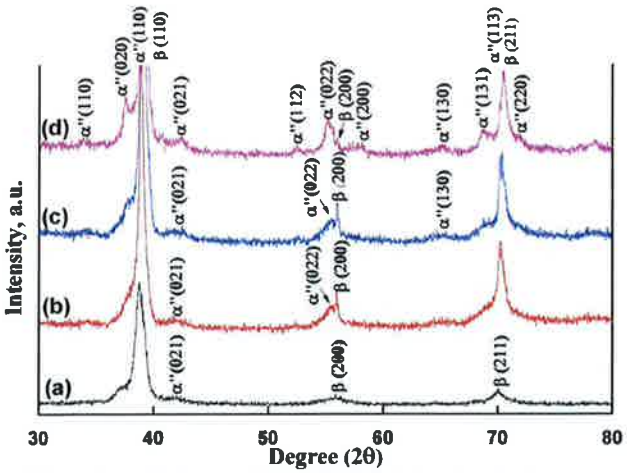

Fig. 5. XRD patterns of (a) the raw material, and the PREP Ti-28Ta powders with the particle size of (b) 150–178 μm, (c) 89–124 μm and (d) 40–65 μm.

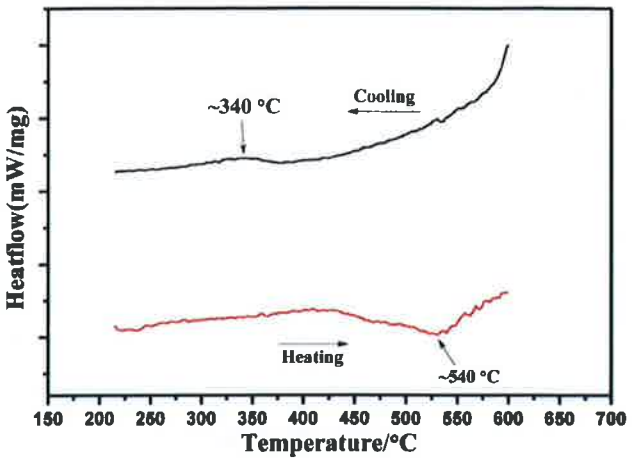

Fig. 7. DSC curves of the PREP Ti-28Ta powders with the particle size range of 40–65 μm.

3.4. Micro-hardness test

Fig. 8 presents the Vickers micro-hardness data of powders with different particle sizes. In general, the micro-hardness of the powders increases with the decrease of particle size. The hardness increases significantly from 148.8 ± 6.7 HV (for the 226 μm particle size) to 164.3 ± 7.1 HV (for the 198 0.8 μm particle size). Decreasing particle size further to 126 μm only causes a slight increase in hardness. For the particle sizes below 126 μm, a further decrease in particle size results in a large hardness increase again. However, the increase of hardness is insignificant when the particle size decreases from 198 to 126 μm.

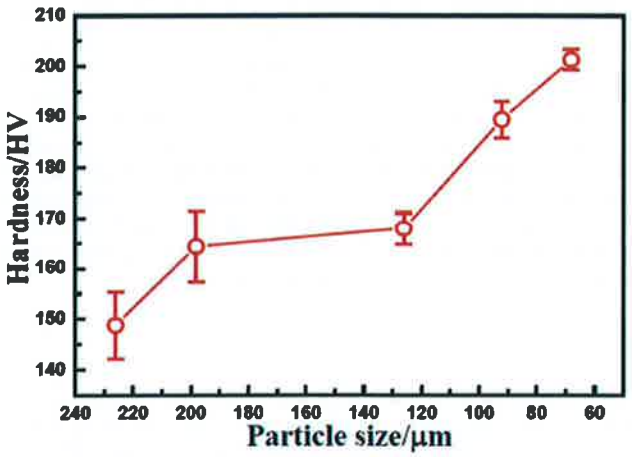

Fig. 8. Vickers micro-hardness of the PREP Ti-28Ta powders as a function of particle size.

4. Discussion

4.1. Rapid cooling effect on particle morphology

It is known that secondary dendrite arm spacing (SDAS), λ, is proportional to the cube root of solidification time (t), as given by Eq. (1) [22,23].

$$\lambda = 5.5(Mt)^{1/3} \quad (1)$$

where M is the coarsening parameter and can be considered constant for a specific alloy. Therefore, equation (1) can be used to estimate the relationship between the cooling rate and particle size by measuring the SDAS. Fig. 9 presents the values of SDAS *vs.* particle size. It is clear that the SDAS in the PREP Ti-28Ta powders decreases with decreasing particle size, suggesting that its cooling rate is inversely proportional to the particle size.

It was reported that during a rapid cooling process, the phase

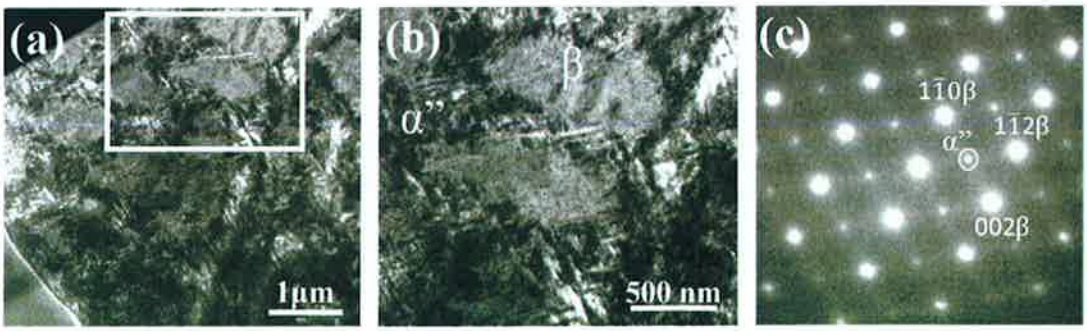

Fig. 6. TEM images and SEAD of the PREP Ti-28Ta powders with the particle size of 40–65 μm. (a) TEM image of the powder, (b) magnified TEM image of the frame in (a), and (c) the corresponding SEAD pattern in (b).

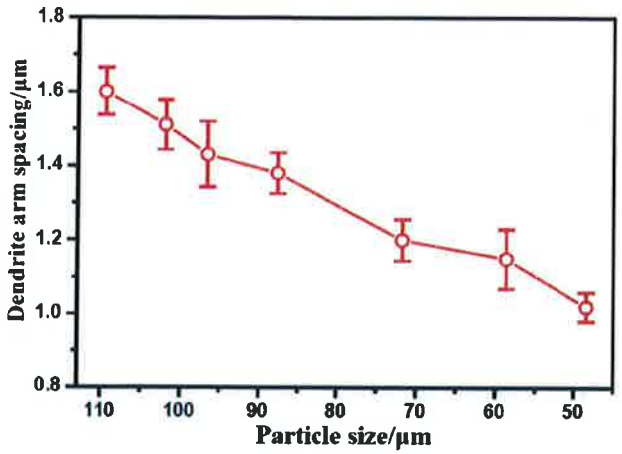

Fig. 9. SDAS as a function of particle size.

constituents and morphology of the solidified powders are a function of particle size [13]. The findings of our study confirm these dependences on particle size, as shown in Figs. 4 and 5. During the atomization, the heat is extracted from a small particle more quickly than the heat from a large particle. Thus, smaller particles experience higher cooling rates. Even within an individual particle, the outermost region will experience a faster cooling than the interior region. As a result, a smaller dendritic microstructure is observed in the outer layer, while larger equiaxed dendritic grains are observed in the center of the powder particles, Fig. 4(a) and (b). In a sufficiently fine particle, the dendritic growth may be strongly suppressed, resulting in a fine dendritic microstructure.

4.2. Martensitic phase transformation

Orthorhombic α" phase is commonly observed in the Ti-Ta alloys. It is formed within the β grain matrix in Ti-Ta alloys when these alloys are either water or gas quenched [2,10]. The XRD, DSC and TEM results (Figs. 5–7) confirm the presence of α" in addition to β. In particular, the XRD analysis estimates that the amount of α" phase increases with decreasing particle size. It is interesting to note that the martensitic α" is preferentially formed at the β grain boundaries, Fig. 6. This phenomenon has not been yet reported in bulk Ti-Ta alloys with the composition around Ti-28Ta [2,10,24]. In these previous studies, the martensitic α" phase was found to emerge within the β grain matrix.

It is speculated that the distortion (stress) occurring at the grain boundaries induces the martensitic transformation from β to α". Such stress-induced martensitic transformations have been well documented for the plastic deformation of β titanium [10,25,26]. It is further suggested that an increased cooling rate intensifies the thermal stress, which in turn intensifies the martensitic transformation. As such, the amount of the martensitic α" phase increases with a decreasing particle size (Fig. 5). The thermal stress may exist across the entire grain; but its magnitude might be larger at grain boundaries and therefore martensitic α" phase preferentially grows at grain boundaries, Fig. 6(b). As noted in the reference data, the martensitic transformation may be constrained by the grain boundaries [27]. Thus, more energy barriers exist to form martensite in a fine-grained alloy. In contrast, we observed that more martensitic α" phase was obtained in parallel with grain refinement in our study. This implies that rapid quenching during PREP not only causes the grain refinement, but also induces a significant thermal stress. Therefore, we assume that the effect of stress-induced martensitic formation outperforms the grain refinement constraint.

4.3. Effect of particle size on micro-hardness

In typical β-type titanium alloys, the hardness of various phases can be rated as [25]: α" < β < ω. The amount of α" within the powders increases with the decrease of particle size. This would cause a hardness reduction. However, grain refinement is accompanied by particle size reduction and rapid cooling leads to a large dislocation density concentration in the solidified powders [13]. Therefore, we conclude that the grain boundary strengthening and high dislocation density in the PREP powders compensate for the α" phase softening.

5. Conclusions

In the present work, we demonstrated production, characterization and micro-hardness properties of spherical Ti-28Ta powders produced *via* PREP. The resultant microstructures, martensitic transformations and micro-hardness of the powders are strongly related to the particle size. The main findings include:

(1) The cooling rate of the PREP Ti-28Ta powders is directly associated with the particle size. Due to the diverse cooling rates in individual particles, large powders exhibited rough morphology and coarse equiaxed dendritic features while small powders demonstrated smooth surface and fine grain structure.
(2) In large particles, the retained metastable β phase is predominant with a small amount of martensitic α". In contrast, α" phase became predominant in addition to β for small particles. A reduced particle size leads to an increased amount of α" and a decreased amount of β phase.
(3) The martensitic ~50 nm wide α" plates were observed to preferentially form at the grain boundaries of the β matrix in fine powders.
(4) The micro-hardness of powders increases with decreasing particle size. This is mainly because of the effects of grain refinement and dislocation increase.

Acknowledgements

We acknowledge the financial support from Shaanxi Science and Technology Co-ordination and Innovation Project (Contract No. 2016KTCQ01-113), Shaanxi Youth Science and Technology New Star Project (Contract No. 2016KJXX-78), and Professor Ma Qian at RMIT University Australia. This work is also supported by the State Key Laboratory for Powder Metallurgy, Central South University, P. R. China. We also acknowledge Mr. Lei Shen and Ms. Jiayi Wen at Northwest Institute for Non-ferrous Metal Research for their technical assistance.

References

[1] K.A. de Souza, A. Robin, Preparation and characterization of Ti–Ta alloys for application in corrosive media, Mater. Lett. 57 (2003) 3010–3016.
[2] Y.L. Zhou, M. Niinomi, T. Akahori, Effects of Ta content on Young's modulus and tensile properties of binary Ti–Ta alloys for biomedical applications, Mater. Sci. Eng. A 371 (2004) 283–290.
[3] D.M. Gordin, E. Delvat, R. Chelariu, G. Ungureanu, M. Besse, D. Laillé, T. Gloriant, Characterization of Ti-Ta alloys synthesized by cold crucible levitation melting, Adv. Eng. Mater. 10 (2008) 714–719.
[4] P.J.S. Buenconsejo, H.Y. Kim, H. Hosoda, S. Miyazaki, Shape memory behavior of Ti–Ta and its potential as a high-temperature shape memory alloy, Acta Mater. 57 (2009) 1068–1077.
[5] Y. Liu, S. Xu, X. Wang, K. Li, B. Liu, H. Wu, H. Tang, Ultra-high strength and ductile lamellar-structured powder metallurgy binary Ti-Ta alloys, JOM 68

(2016) 899–907.
[6] S.J. Savage, F.H. Froes, Production of rapidly solidified metals and alloys, JOM 36 (1984) 20–33.
[7] S. Hata, K. Oki, T. Hashimoto, N. Kuwano, Microstructures of Ti50Al45Mo5 alloy powders produced by plasma rotating electrode process, JPE 22 (2001) 386–393.
[8] Y. Liu, X. Liang, B. Liu, W. He, J. Li, Z. Gan, Y. He, Investigations on processing powder metallurgical high-Nb TiAl alloy sheets, Intermetallics 55 (2014) 80–89.
[9] K.A. Bywater, J.W. Christian, Martensitic transformations in titanium-tantalum alloys, Philos. Mag. 25 (1972) 1249–1273.
[10] R.W. Margevicius, J.D. Cotton, Stress-assisted transformation in Ti-60 wt pct Ta alloys, Metall. Mater. Trans. A 29 (1998) 139–147.
[11] T.F. Broderick, A.G. Jackson, H. Jones, F.H. Froes, The effect of cooling conditions on the microstructure of rapidly solidified Ti-6Al-4V, MTA 16 (1985) 1951–1959.
[12] R. Yamanoglu, R.M. German, S. Karagoz, W.L. Bradbury, M. Zeren, W. Li, E.A. Olevsky, Microstructural investigation of as cast and PREP atomised Ti-6Al-4V alloy, Powder Metall. 54 (2011) 604–607.
[13] D.-Y. Yang, S. Guo, H.-X. Peng, F.-Y. Cao, N. Liu, J.-F. Sun, Size dependent phase transformation in atomized TiAl powders, Intermetallics 61 (2015) 72–79.
[14] A.M. Birt, V.K. Champagne Jr., R.D. Sisson Jr., D. Apelian, Microstructural analysis of Ti–6Al–4V powder for cold gas dynamic spray applications, Adv. Powder Technol. 26 (2015) 1335–1347.
[15] J.D. Cotton, J.F. Bingert, P.S. Dunn, R.A. Patterson, Microstructure and mechanical properties of Ti-40 Wt Pct Ta (Ti-15 At. Pct Ta), Metall. Mater. Trans. A 25 (1994) 461–472.
[16] D.H. Ping, Y. Mitarai, F.X. Yin, Microstructure and shape memory behavior of a Ti–30Nb–3Pd alloy, Scr. Mater. 52 (2005) 1287–1291.
[17] X.H. Zheng, J.H. Sui, X. Zhang, Z.Y. Yang, H.B. Wang, X.H. Tian, W. Cai, Thermal stability and high-temperature shape memory effect of Ti–Ta–Zr alloy, Scr. Mater. 68 (2013) 1008–1011.
[18] Y. Cui, Y. Li, K. Luo, H. Xu, Microstructure and shape memory effect of Ti–20Zr–10Nb alloy, Mater. Sci. Eng. A 527 (2010) 652–656.
[19] X.H. Zheng, J.H. Sui, X. Zhang, X.H. Tian, W. Cai, Effect of Y addition on the martensitic transformation and shape memory effect of Ti–Ta high-temperature shape memory alloy, J. Alloys Compd. 539 (2012) 144–147.
[20] L.W. Ma, H.S. Cheng, C.Y. Chung, B. Yuan, Effect of heat treatment time on microstructure and mechanical properties of Ti–19Nb–9Zr (at%) shape memory alloy, Mater. Sci. Eng. A 561 (2013) 427–433.
[21] P. Xue, Y. Li, F. Zhang, C. Zhou, Shape memory effect and phase transformations of Ti–19.5Zr–10Nb–0.5Fe alloy, Scr. Mater. 101 (2015) 99–102.
[22] W. Kurz, D.J. Fisher, Fundamentals of Solidification, Trans Tech Publications, 1989.
[23] A. Ilbagi, H. Henein, 3D Quantitative characterization of rapidly solidified Al-36 wt pct Ni, Metallurgical Mater. Trans. A 45 (2014) 2152–2160.
[24] J. Zhang, R. Rynko, J. Frenzel, C. Somsen, G. Eggeler, Ingot metallurgy and microstructural characterization of Ti–Ta alloys, Int. J. Mater. Res. 105 (2013) 156–167.
[25] L.X. Yin, S.X. Liang, L.Y. Zheng, M.Z. Ma, R.P. Liu, Inhibition of martensitic formation and mechanical properties of the TZ20 alloy during hot rolling, J. Alloys Compd. 649 (2015) 726–730.
[26] Z. Li, B. Zheng, L. Kurmanaeva, Y. Zhou, R.Z. Valiev, E.J. Lavernia, High-strain induced reverse martensitic transformation in an ultrafine-grained Ti-Nb-Ta-Zr alloy, Philos. Mag. Lett. 96 (2016) 189–195.
[27] P. La Roca, L. Isola, P. Vermaut, J. Malarría, Relationship between martensitic plate size and austenitic grain size in martensitic transformations, Appl. Phys. Lett. 106 (2015) 221903.